KLOE-2

The KLOE-2 Collaboration at the LNF

D. Babusci, G. Bencivenni, C. Bloise (Resp), F. Bossi, G. Capon (Ass.), P. Ciambrone,
E. Dané (Art. 23), E. De Lucia, A. De Santis (Art.23), P. De Simone, D. Domenici, G. Felici,
G. Fortugno (Tec.), S. Giovannella, M. Iannarelli (Tec.), M. Martini (Ass)*,
M. Mascolo (PostDoc), S. Miscetti, G. Morello (PostDoc), A. Palladino (PostDoc),
R. Rosellini (Tec.), P. Santangelo, I. Sarra (PostDoc), F. Sborzacchi (Tec.), G. Venanzoni.

In collaboration with "LNF-SEA"
A. Balla, M. Beretta, M. Carletti, G. Corradi, U. Denni, A. Frani, M. Gatta, G. Papalino

**Also Dipartimento di Scienze e Tecnologie applicate, "Guglielmo Marconi" University, Rome, Italy*

1 DAFNE Operation and KLOE-2 Run

During 2015 both KLOE-2 and DAFNE successfully demonstrated the feasibility of a long term acquisition program with the Run-I data taking campaign, ending in July 2015 with 1 fb^{-1} integrated luminosity. Record performance in terms of 2x10^{32} cm^{-2}s^{-1} peak luminosity and 12 pb^{-1} maximum daily integrated luminosity were achieved with the innovative crab-waist beam collision scheme, developed in Frascati, that will be employed in the upgrade of the B-factory currently under construction at the KEK Laboratory in Japan and is considered a valid option in several future projects.

The collider uptime and the integrated luminosity have been very satisfactory, thanks to a strong consolidation program and a fruitful collaboration between DAFNE and KLOE-2 teams, and therefore the prospects for the KLOE-2 collaboration to pursue a successful data taking campaign very positive. Run-II started in November 2015 aiming at a total delivered luminosity of 2.5 fb^{-1} by July 2016.

The KLOE-2 data taking campaign will allow to perform CPT symmetry and quantum coherence tests using neutral kaons with an unprecedented precision, high precision studies of $\gamma\gamma$-physics processes like $e^+e^- \to e^+e^-\pi^0$ ($\gamma\gamma \to \pi^0$), and the search for new exotic particles that could constitute the dark matter, among the fields to be addressed.

2 Commissioning Detector Upgrades

The general purpose KLOE detector, composed by one of the biggest drift chambers ever built surrounded by a lead-scintillating fiber electromagnetic calorimeter among the best ones for energy and timing performance at low energies, undergone several upgrades including State-of-The-art cylindrical GEM detector, the Inner Tracker, to improve vertex reconstruction capabilities near the interaction region. To study $\gamma\gamma$-physics the detector has been upgraded with two pairs of electron-positron taggers: the Low Energy Tagger (LET), inside the KLOE apparatus, and the High Energy Tagger (HET) along the beam lines outside the KLOE detector.

Along with Run-I data taking, the commissioning of the detector upgrades has been progressing together with the software development needed for the reconstruction and simulation of the upgraded KLOE-2 detector. The new accelerator configuration with increased trigger rate and machine background contamination with respect to the KLOE run, although sustainable, required the development of a new strategy for data selection and data reduction. First calibration of the new detectors were obtained including the Inner Tracker. KLOE-2 is the first high-energy experiment using the GEM technology with a cylindrical geometry, a novel idea that was developed at LNF exploiting the kapton properties to build a transparent and compact tracking system. Alignment and calibration of this detector was never done before and represents one of the challenging activities of the experiment. Preliminary results with cosmic-ray muons acquired with and without magnetic field are within expectations for the Inner Tracker resolution

The HET operability at DAFNE has been established with dedicated runs to characterize its stations in terms of time resolution and efficiency, and setting up first level calibration. The DAFNE bunch structure has been successfully measured. First studies of the contributions to the HET total rate have been performed: the main component is given by Bhabha scattering together with a contribution from Touschek scattering.

3 Physics achievements

Together with the activities related to the new KLOE-2 run, several analysis are ongoing on the KLOE data set both in kaon and hadron physics sectors. New limits on the U-boson searches in the dark sector are among the main physics results achieved this year: i) using the final state $e^+e^- \to U\gamma$, U$\to$ e^+e^- we improved the exclusion region of the parameters space allowed by the discrepancy between the observed and predicted (g-2)$_\mu$ down to 5 MeV U-boson mass mU values [?], ii) we searched for the evidence of a Higgsstrahlung process in the invisible dark Higgs scenario leading to a final state with a dark photon U and a dark Higgs boson h, with U decaying into a muon pair and h producing a missing energy signature [?].

3.1 Limit on the production of a low-mass vector boson in $e^+e^- \to U\gamma$, U$\to$ e^+e^- with the KLOE experiment

The existence of a new force beyond the Standard Model is compelling because it could explain several striking astrophysical observations which fail standard interpretations, such as neutrino oscillations and the measured anomalous magnetic moment of the muon. With the KLOE detector we searched for the light vector mediator of this dark force, the U boson, studying the process $e^+e^- \to U\gamma$, U$\to$ e^+e^-, and using radiative return to search for a resonant peak in the dielectron invariant-mass distribution m$_{ee}$. This search differs from the previous KLOE results [?, ?, ?] in its capability to probe the low mass region close to the dielectron mass threshold.

We selected events with three separate calorimeter energy deposits corresponding to two oppositely-charged lepton tracks and a photon. The final-state electron, positron, and photon were required to be emitted at large angle $55^o < \theta < 125^o$ with respect to the beam axis, such that they are explicitly detected in the barrel of the calorimeter. The irreducible background originates from the $e^+e^- \to e^+e^-\gamma$ radiative Bhabha scattering process, having the same three final-state particles. The large-angle selection greatly suppresses the t-channel contribution from the irreducible Bhabha-scattering background which is strongly peaked at small angle.

To estimate the level of background contamination MonteCarlo event generators interfaced with the full KLOE detector simulation, GEANFI [?], including detector resolutions and beam conditions on a run-by-run basis, has been used and a modified version of the Babayaga-NLO event generator implemented within GEANFI in order to evaluate the U-boson selection efficiency. Excluding the irreducible background from radiative Bhabha scattering events, the contamination from the sum of residual backgrounds after all analysis cuts is less than 1.5% in the whole m$_{ee}$ range, and none of the background shapes are peaked, eliminating the possibility of a background mimicking the resonant U-boson signal. The irreducible Bhabha scattering background was simulated using the Babayaga-NLO [?] event generator implemented within GEANFI including the s-, t-, and s-t interference channels.

We found no evidence for a U-boson resonant peak in the process $e^+e^- \to U\gamma$, U$\to e^+e^-$ using the radiative return method and an integrated luminosity of 1.54 fb^{-1}. The CLs technique [?] has been used to determine the limit on the number of signal U-boson events, $\mathrm{N_U}$, at 90% confidence level using the m_{ee} distribution. We then translated the limit on $\mathrm{N_U}$ to a 90% confidence level limit on the kinetic mixing parameter as a function of m_{ee} as done in our previous analysis [?]. A 90% CL upper limit on the kinetic mixing parameter ϵ^2 at 10^{-6} 10^{-4} in the U-boson mass range 5520 MeV/c^2 approaching the dielectron mass threshold has been set. This limit partly excludes some of the remaining parameter space in the low dielectron mass region allowed by the discrepancy between the observed and predicted (g-2)$_\mu$.

Our limit is shown in Fig. **??** along with the indirect limits from the measurements of (g-2)$_e$ and (g-2)$_\mu$ at 5σ shown with dashed curves. Limits from the following direct searches are shown with shaded regions and solid curves: E141 [?], E774 [?], KLOE($\phi \to \eta U, U \to e^+e^-$) [?, ?], Apex [?], WASA [?], HADES [?], A1 [?], KLOE($e^+e^- \to U\gamma$, U $\to \mu^+\mu^-$) [?], BaBar [?], and NA48/2 [?].

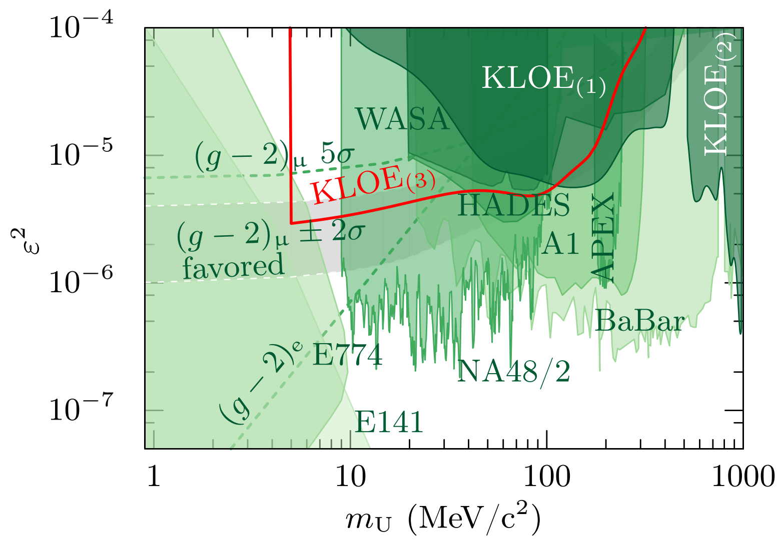

Figure 1: Exclusion limits on the kinetic mixing parameter squared, ϵ^2, as a function of the U-boson mass. The red curve labeled KLOE$_{(3)}$ is the result of this article while the curves labeled KLOE$_{(1)}$ and KLOE$_{(2)}$ indicate the previous KLOE results. Also shown are the exclusion limits provided by E141, E774, Apex, WASA, HADES, A1, BaBar, and NA48/2. The gray band delimited by the dashed white lines indicates the mixing level and mU parameter space that could explain the discrepancy observed between the measurement and SM calculation of the muon (g-2)$_\mu$.

3.2 Search for dark Higgsstrahlung in $e^+e^- \to \mu^+\mu^-$ and missing energy events with the KLOE experiment

The U-boson can be produced at e^+e^- colliders via different processes: $e^+e^- \to U\gamma$, $e^+e^- \to Uh'$ (dark Higgsstrahlung) and in decays of vector particles to pseudoscalars. The process $e^+e^- \to Uh'$, with the U-boson decaying into lepton or hadron pairs, is an interesting reaction to be studied at an e^+e^- collider, being less suppressed, in terms of the mixing parameter, than the other final states listed above. We have studied the Higgsstrahlung process $e^+e^- \to Uh'$ using KLOE data collected both at the center of mass energy of $\sim$ 1019 MeV, the mass of the ϕ-meson (1.65 fb^{-1} on-peak sample), and at a center of mass energy of $\sim$ 1000 MeV (0.206 fb^{-1} off-peak sample). The search has been limited to the decay of the U-boson into a muon pair: the final state signature is then a pair of opposite charge muons plus missing energy. The measurement is thus performed in the range $2m_\mu < m_U < 1000$ MeV with the constraint $m_{h'} < m_{\mathrm{U}}$.

The Monte Carlo simulation of the signal process $e^+e^- \to Uh'$ has been produced using an ad hoc generator interfaced with the standard KLOE simulation program ?). Signal samples have been generated for various pairs of $m_{h'}$ - m_{U} values along a grid with steps of $\sim$ 30 MeV to cover all the allowed kinematic region. The signal process signature would thus be the appearance of a sharp peak in the bidimensional distribution $M_{\mu\mu}$-M_{miss}. The distribution of the polar angle direction of the muon pair momentum, θ, contrarily to most of the dominant background processes, is expected to prefer large angles. Therefore the angular distribution allows to reject most of the background of QED processes with a simple geometrical selection. The calorimeter hermeticity has been exploited as photon veto and a particle identification (PID) algorithm was applied to the two tracks, based on the calorimeter excellent energy and time resolutions and trained on simulated Monte Carlo samples to perform muon to electron discrimination.

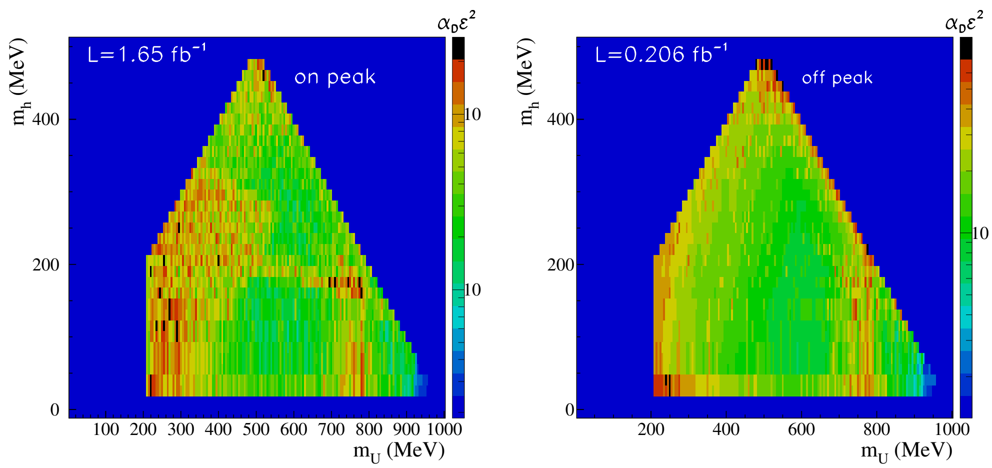

Figure 2: 90% CL upper limits in $\alpha_D \times \epsilon^2$ for the on-peak sample (left plot) and off-peak sample (right plot).

As no evidence of the dark Higgsstrahlung process was found, 90% confidence level Bayesian upper limits on the number of events were derived bin by bin in the $M_{\mu\mu}$-M_{miss} plane, separately for the on-peak and off-peak samples, and then converted in terms of $\alpha_D \times \epsilon^2$ (Fig.**??**). Figure **??** shows the combined on-peak and off-peak 90% CL upper limits projected along the m_U and $m_{h'}$ axes, with the different curves in m_U ($m_{h'}$) corresponding to different values of $m_{h'}$ (m_U). Values as low as $10^{-9}\div10^{-8}$ of the product $\alpha_D \times \epsilon^2$ are excluded at 90% CL in the range $2m_\mu < m_U <$ 1000 MeV with $m_{h'} < m_U$.

3.3 Study of the Dalitz decay $\phi \to \eta e^+e^-$ with the KLOE detector

The vector to pseudoscalar transition form factor are not well described by the Vector Meson Dominance (VMD) model, as in the case of the process $\omega \to \pi^0\mu^+\mu^-$, measured by the NA60

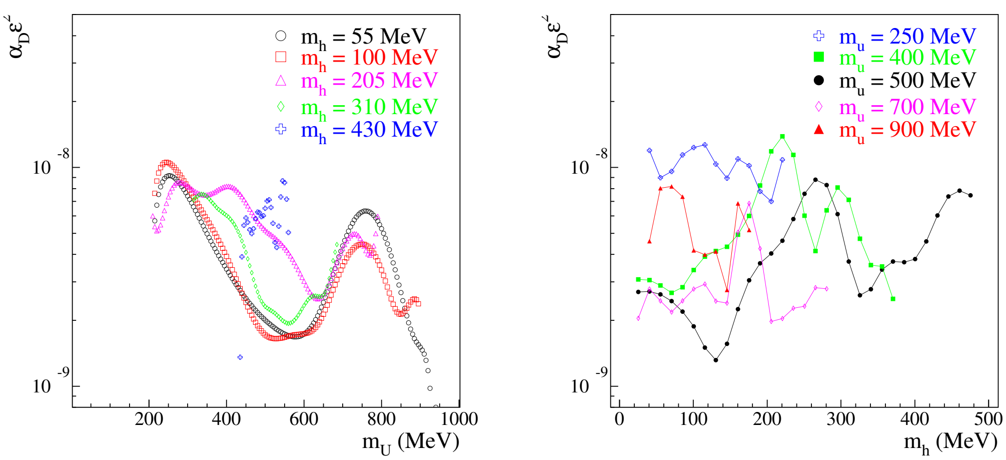

Figure 3: Combined 90% CL upper limits in $\alpha_D \times \epsilon^2$ as a function of m_U for different values of $m_{h'}$ (top plot) and as a function of $m_{h'}$ for different values of m_U (bottom plot).

collaboration **?**). New measurements of other $V \to P\gamma^*$ transitions are therefore needed to confirm this evidence. The only other existing experimental result comes from the SND experiment, which has measured the M_{ee} invariant mass distribution of the $\phi \to \eta e^+e^-$ decay on the basis of 213 events **?**). The measurement of the form factor slope, $b_{\phi\eta} = (3.8 \pm 1.8)\,\mathrm{GeV}^{-2}$, differs by $1.6\,\sigma$'s from the VMD expectations ($b_{\phi\eta} = 1\,\mathrm{GeV}^{-2}$). At KLOE, a detailed study of the $\phi \to \eta e^+e^-$ decay has been performed with 1.7 fb^{-1}, using the $\eta \to \pi^0\pi^0\pi^0$ final state. At the end of the analysis chain, 30,577 events are selected, with a residual background contamination of $\sim 3\%$. In Fig. **??**

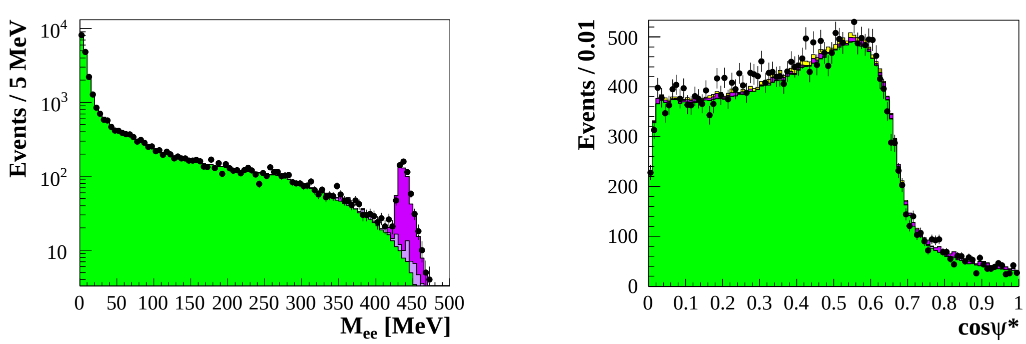

Figure 4: $\phi \to \eta e^+e^-$: data-MC comparison for the di-lepton invariant mass (left) and the cosψ^* variable (right) at the end of the analysis chain.

the comparison between data and Monte Carlo distributions at the end of the analysis chain is shown. After background subtraction, the measured branching fraction for the $\phi \to \eta e^+e^-$ process is:

$$BR(\phi \to \eta e^+e^-) = (1.075 \pm 0.007 \pm 0.038) \times 10^{-4}\,, \tag{1}$$

much more precise compared to the present PDG average of $(1.15 \pm 0.10) \times 10^{-4}$. The slope of the transition form factor, $b_{\phi\eta}$, has been obtained from a fit to the di-lepton invariant mass using the decay parametrization from Ref. [?]:

$$b_{\phi\eta} = (1.17 \pm 0.10\,^{+0.07}_{-0.11}\,)\ \mathrm{GeV}^{-2}\,, \tag{2}$$

the result is in agreement with VMD predictions. As cross check, we have also fit the modulus square of the transition form factor $|F_{\phi\eta}(q^2)|^2$ as a function of the invariant mass of the electron positron pair. The distribution of the modulus squared of the transition form factor (Fig. **??**) has been obtained by dividing the M_{ee} spectrum bin by bin with the corresponding distribution obtained for MC events generated with a constant transition form factor. The value of $b_{\phi\eta}$ extracted from the fit is in agreement with Eq. (**??**).

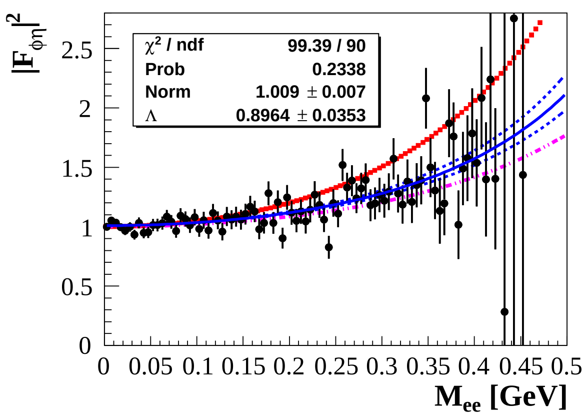

Figure 5: $\phi \to \eta e^+e^-$: $\phi\eta$ form factor as a function of the di-lepton invariant mass. The blue curve is the fit result, with its uncertainty, while in red and pink expectations from VMD and ref. [?] are reported, respectively.

References

1. A. Anastasi et al., KLOE-2 Collaboration, Phys. Lett. B 750 (2015) 633–637
2. D. Babusci et al., KLOE-2 Collaboration, Phys. Lett. B 747 (2015) 365–372
3. F. Archilli et al., KLOE-2 Collaboration, Phys. Lett. B 706 (2012) 251–255.
4. D. Babusci et al., KLOE-2 Collaboration, Phys. Lett. B 720 (2013) 111–115.
5. D. Babusci et al., KLOE-2 Collaboration, Phys. Lett. B 736 (2014) 459–464.
6. F. Ambrosino et al., KLOE-2 Collaboration, Nucl. Instrum. & Methods 534 (2004) 403.

7. L. Barzè, et al., Eur. Phys. J. C 71 (2011) 1680. G. Balossini, et al., Nucl. Phys. B 758 (2006) 227. C. M. C. Calame, Phys. Lett. B 520 (2001) 16. C. M. C. Calame, et al., Nucl. Phys. B 584 (2000) 459.

8. G. C. Feldman, R. D. Cousins, Phys. Rev. D 57 (1998) 3873.

9. J. D. Bjorken, et al., Phys. Rev. D 80 (2009) 075018.

10. S. Abrahamyan et al., APEX Collaboration, Phys. Rev. Lett. 107 (2011) 191804.

11. P. Adlarson et al., WASA-at-COSY Collaboration, Phys. Lett. B 726 (2013) 187.

12. G. Agakishiev et al., HADES Collaboration, Phys. Lett. B 731 (2014) 265–271.

13. H. Merkel et al., A1 Collaboration, Phys. Rev. Lett. 112 (2014) 221802.

14. J.P. Lees et al., BaBar Collaboration, Phys. Rev. Lett. 113 (2014) 201801.

15. J.R. Batley et al., NA48/2 Collaboration, Phys. Lett. B 746 (2015) 178–185.

16. S. Damjanovic et al. Na60 collaboration, Phys. Lett. B 677 (2009) 260.

17. M. N. Achasov et al., SND Collaboration, Phys. Lett. B 504 (2001) 275.

18. L.G. Landsberg, Phys. Rep. 128 (1985) 301.

19. C. Terschlusen and S. Leupold, Phys. Lett. B 691 (2010) 191.